



Repeated penetration and different depth explosion of ultra-high performance concrete



Jianzhong Lai^{*}, Xujia Guo, Yaoyong Zhu

School of Materials Science and Engineering, Nanjing University of Science and Technology, Nanjing 210094, China

ARTICLE INFO

Article history:

Received 30 August 2014

Received in revised form

5 May 2015

Accepted 8 May 2015

Available online 19 May 2015

Keywords:

Ultra-high performance concrete

Penetration

Explosion

Damage

Finite element

ABSTRACT

Ultra-high performance concrete (UHPC) was prepared and its dynamic behavior was researched under repeated penetration and different depth explosion using 14.5 mm bullets and TNT explosives. The penetration depth of UHPC was measured on different number of penetrations. The damage of UHPC was measured by the ultrasonic wave velocity method and the penetration process of UHPC was observed by the high-speed camera. The explosion damage of UHPC with TNT explosive embedded at different depths was measured and the explosion process was simulated by the finite element method. Results show that UHPC resistance to repeated penetration and different depth explosion is improved significantly by hybrid reinforcement of steel and basalt fibers. The second penetration depth of UHPC with basalt coarse aggregates is decreased and the damage of UHPC with basalt coarse aggregates is more than that of UHPC without basalt coarse aggregates. The mass and the placing depth of explosive have important effects on the damage of UHPC.

© 2015 Elsevier Ltd. All rights reserved.

1. Introduction

Underground works will suffer attacks by the precision guided penetration weapons. So it is an urgent problem to improve the resistant ability of protective structures against repeated impact and different depth explosion. Forrestal and Tzou [1] proposed a concrete penetration resistance model by using the spherical cavity expansion theory and the predictions from the model are in good agreement with penetration depth data from experiments. Gomez and Shukla [2] conducted a series of experiments on multiple impact penetration into semi-infinite concrete and proposed an empirical equation to calculate the multiple penetration depth in relation to the modifying factor and shot number. Almansa and Canovas [3] proposed a model to predict the thickness needed to avoid perforation or scabbing and to obtain the residual velocity by researching the behavior of normal and steel fiber reinforced concretes under impact of small projectiles. Teng et al. [4] proposed a simplified model to perform finite element analyses on reinforced concrete subjected to impact and the computational results using this model were very close to the test data. Almusallam et al. [5] researched the effectiveness of hybrid fibers in improving the

impact resistance of concrete slabs. The test results showed that the hybrid fibers in the concrete led to smaller crater volumes and reduced the spalling and scabbing damage. Tabatabaei et al. [6] conducted a series of tests to compare the blast resistance of panels constructed with either conventional reinforced concrete (RC) or long carbon fiber reinforced concrete (LCFRC). Results showed that the addition of long carbon fibers significantly increased the concrete's blast resistance and significantly reduced the degree of cracking associated with the concrete panels. Zhou et al. [7] used a dynamic plastic damage model for concrete material to estimate the responses of both an ordinary reinforced concrete slab and a high strength steel fiber concrete slab subjected to blast loading. Comparison of numerical results with the experimental results showed that the present model gave reliable prediction of blast pressure and damage from the first blast but could not give an accurate estimation of blast pressure on the slab from a second blast.

Ultra-high performance concrete (UHPC) has ultra-high strength, high toughness and high durability. Therefore, it is an ideal selection for building protective structure. Yu et al. [8] designed an Ultra High Performance Fiber Reinforced Concrete (UHPFRC) with a relatively low binder amount by utilizing the improved packing model. The maximum compressive and flexural strengths at 28 days of the obtained UHPFRC were about 150 MPa and 30 MPa respectively. Wang et al. [9] assessed the

^{*} Corresponding author. Tel.: +86 13770574619.
E-mail address: jzh-lai@163.com (J. Lai).

durability of UHPFRC after accelerated aging using gas permeability under varying confinement and the UHPFRC properties were compared to those of standard mortar and ordinary concrete. Habel et al. [10] studied the development of the mechanical properties for UHPFRC between 3 and 365 days. Results showed that the rate of development of mechanical properties was highest for the secant modulus, followed by the compressive and then the tensile strength. Oertel et al. [11] compared the effects of different silica types on the hydration in ultra-high performance concrete. Results indicated that silica fume and pyrogenic silica accelerated alite hydration by increasing the surface for nucleation of C-S-H phases. Tuan et al. [12] studied the effect of rice husk ash (RHA) on the hydration and microstructure development of UHPC. The results showed that the addition of RHA increased the degree of cement hydration in UHPC at later ages and refined the pore structure of UHPC and reduced the $\text{Ca}(\text{OH})_2$ content. Kang and Kim [13] investigated the effect of the fiber orientation distribution on the tensile behavior of Ultra High Performance Fiber Reinforced Cementitious Composites (UHPFRCC). Results showed that the effect was very small on pre-cracking behavior, but was significant on post-cracking behavior of UHPFRCC.

Protective structure built with UHPC has excellent ability against penetration, impact and explosion. Millard et al. [14] investigated the dynamic increase factor (DIF) under flexural and shear high-speed loading of ultra high performance fibre reinforced concrete. The results show that the DIF of the flexural tensile strength is rising from 1.0 at 1 s^{-1} but no DIF should be used to increase the shear strength at high loading rates. Maca et al. [15] researched the mix design of UHPFRC and its response to deformable and non-deformable projectile impact. The magnitude of the damage was assessed based on the penetration depth, crater diameter and loss of mass. Riedel et al. [16] conducted an experimental series on UHPC panels subjected to aircraft engine impact. The material's high compressive strength reduced the effect of the front side missile penetration without significant spalling. The mechanical effects of fibers reduce damage to the panel rear side and increase the ballistic limit velocity. Ellis et al. [17] investigated the behavior of UHPC panels subjected to planar waveforms with specific impulses between 0.77 and 2.05 MPa-ms and the experimental results were used to validate a multiscale model which accounts for structure and phenomena at two length scales. Yi et al. [18] performed blast tests on reinforced ultra-high strength concrete (UHSC) and reactive powder concrete (RPC) panels to evaluate their resistance to terrorist attacks or accidental impacts. The results showed that UHSC and RPC have better blast explosion resistance than normal strength concrete. Mao et al. [19] presented a numerical investigation on the performance of UHPFRC under blast loading with a concrete material model which takes into account the strain rate effect. The performance of the numerical models

was verified by comparing simulation results to the data from corresponding full scale blast tests.

In this paper, UHPC was prepared by different fibers reinforcement and replacing cement with large amount of ultra-fine industrial waste powders. The resistance of UHPC subjected to repeated penetration and different depth explosion was researched using 14.5 mm bullets and TNT explosive. The penetration depth and damage of concrete targets were measured after impact of penetration and blast.

2. Materials and methods

The cylindrical targets of UHPC were 300 mm in the diameter and 300 mm in the length. The targets were cast inside cylindrical steel molds with the thickness of 1.6 mm. The mix proportions of UHPC are shown in Table 1. All the targets were prepared by the following raw materials: Portland cement, silica fume, blast-furnace slag powder, superplasticizer, natural sand, coarse aggregate and fibers. The mortar compressive strength is no less than 52.5 MPa on 28 d for the Portland cement according to the Chinese national standard GB175-2007. The specific surface areas of the silica fume and blast-furnace slag powder are $22000 \text{ m}^2/\text{kg}$ and $1000 \text{ m}^2/\text{kg}$ respectively. The water-reducing ratio of the polycarboxylate based superplasticizer is more than 40%. The maximum particle sizes of the natural sand and basalt coarse aggregate are 2.5 mm and 16 mm respectively. The fineness modulus of the natural sand is 2.6. The length and diameter of the copper coated steel fiber are 13 mm and 0.2 mm. The length and diameter of the basalt fiber are 20 mm and $17 \mu\text{m}$.

The penetration experiments were carried out using the 14.5 mm standard bullets and the 14.5 mm gun. The bullets were shot into the targets perpendicularly. The mass, the diameter and the length of the bullet are 43 g, 14.8 mm and 52 mm respectively. The device of penetration is shown in Fig. 1 including the gun, tinfoil target, time-meter, high speed camera, concrete target and back plate.

The dimension of the targets for blast is same as that of the targets for penetration. A cylindrical hole with the size of $\Phi 38 \text{ mm} \times 150 \text{ mm}$ was prefabricated in the center of the target for placing different depth explosives as shown in Fig. 2. The cylindrical TNT explosive with the diameter of 37 mm was embedded inside the hole. The length of the cylindrical TNT explosive varied with the mass. Two kind of buried depth of TNT explosive are selected (150 mm and 50 mm) in order to analyze the influence of buried depth on the behavior of ultra-high performance concrete subjected to blasting. The dimension and mass of the TNT explosives for different targets are shown in Table 6 and 7.

Table 1
Mix proportions of UHPC.

Materials	Binder(wt%)			S/b	G/b	Sp/b	W/b	$V_{\text{SF}}(\%)$	$V_{\text{BF}}(\%)$	f_c (MPa)
	Cement	Silica fume	Slag							
M2	50	20	30	1.2	0	0.02	0.18	0	0	124
M2SF3	50	20	30	1.2	0	0.02	0.18	3	0	232
M2SF3BF1	50	20	30	1.2	0	0.02	0.18	3	1	234
GM2SF3	50	20	30	0.6	0.6	0.02	0.18	3	0	248
GM2SF3BF1	50	20	30	0.6	0.6	0.02	0.18	3	1	251

Note: S/b: the mass ratio of sands to binder, G/b: the mass ratio of coarse basalt aggregates to binder, Sp/b: the mass ratio of superplasticizer to binder, w/b: the mass ratio of water to binder, V_{SF} : the volume fraction of steel fibers, V_{BF} : the volume fraction of basalt fibers, f_c : static compressive strength of UHPC cured in 20°C water for 3 d and then in 95°C water for 24 h).

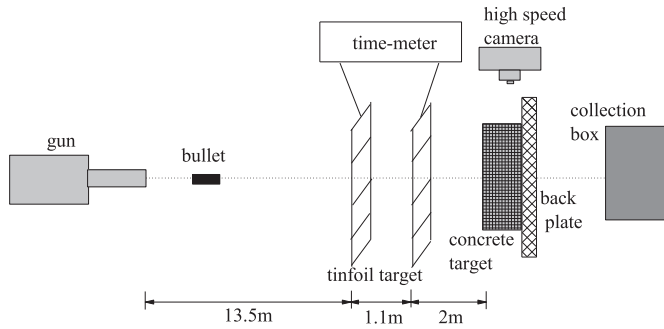


Fig. 1. The device of penetration experiments.



Fig. 2. Concrete target for different depth explosion (The cylindrical hole in the middle of the target is used for placing explosive).

3. Results and analysis of repeated penetration experiments

3.1. Fracture pattern and penetration depth of UHPC targets

The damage of different targets subjected to the first penetration is shown in Table 2 and Fig. 3. Results show that the concrete matrix M2 is cracked completely while the fiber reinforced targets have less damage and little spalling in the front sides and no crack on the rear sides. The penetration resistance of fiber reinforced materials is better than that of matrix because the fibers have the effect of preventing cracking. The size and number of micro-cracks in the targets without coarse aggregates are much smaller than those in the targets with coarse aggregates. So the damage of the targets without coarse aggregates is less than that of the targets with coarse aggregates.

The targets were shot for the second time and the second shooting point on the targets was as same as the first one. The damage of the different targets subjected to the second penetration is shown in Table 3 and Fig. 4. Results show that large spalling appeared on the front side of the targets subjected to the second penetration and the penetration depth increased gradually. The increase of the penetration depth is 46.7%, 51.8%, 23.0%, 13.5% respectively for M2SF3, M2SF3BF1, GM2SF3, GM2SF3BF1 on the second penetration compared with those on the first penetration. The bullets were still inside the targets and did not perforate the targets. Only target M2SF3BF1 had no crack on the rear side and it was shot for the third time. The damage of target M2SF3BF1 subjected to the third penetration is shown in Table 4 and Fig. 5. Results show that the front side of target M2SF3BF1 had small cracks and spalling and there was still no damage on the rear side.

As shown in Figs. 3 and 4, the bonding between the concretes and the steel cylinders was well on the first time of penetration

Table 2
Materials damage of the targets subjected to the first penetration.

Materials of targets	Bullet speed(m/s)	Penetration depth(mm)	Damage of the targets
M2	945	242	Crushed completely
M2SF3	960	165	One deep crack on the front side and many small cracks on the rear side
M2SF3BF1	979	135	Crushed locally on the front side and no visible crack on the front and rear side
GM2SF3	1002	183	Four deep cracks on the front side and no visible crack on the rear side
GM2SF3BF1	978	178	Five deep cracks on the front side and no visible crack on the rear side

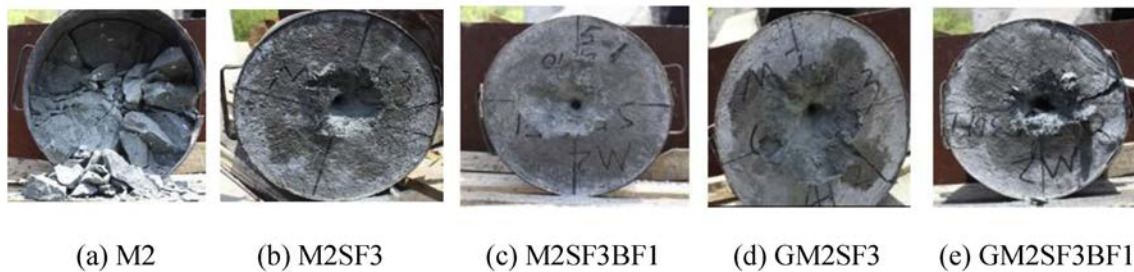


Fig. 3. Damage on the front side of the targets subjected to the first penetration.

Table 3
Materials damage of the targets subjected to the second penetration.

Materials of targets	Bullet speed(m/s)	Penetration depth(mm)	Damage of the targets
M2SF3	970	242	Crushed locally and many cracks on the front side and many small cracks on the rear side
M2SF3BF1	968	205	Crushed locally and many cracks on the front side and no crack on the rear side
GM2SF3	1008	225	Crushed locally and many cracks on the front side and two cracks on the rear side
GM2SF3BF1	985	202	Crushed locally and many cracks on the front side

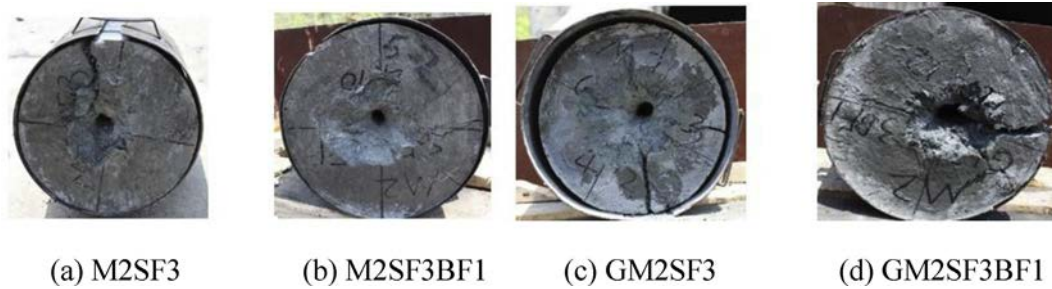


Fig. 4. Damage on the front of the targets subjected to the second penetration.

Table 4

Materials damage of the target subjected to the third penetration.

Materials of target	Bullet speed(m/s)	Penetration depth(mm)	Damage of the targets
M2SF3BF1	970	272	Crushed locally and many cracks on the front side and no obvious crack on the rear side



(a) Front side of the target



(b) Rear side of the target

Fig. 5. Damage the target M2SF3BF1 subjected to the third penetration.

while some of the concretes were separated from the steel cylinders on the second time of penetration. The reason is that the damage of concretes and the deformation of steel lining were improved obviously and the interface between concrete and steel was destroyed by stress wave on the second time of impact.

Elshenawy and Li [20] Found that the increase of concrete strength led to large decrease of the OWP jet penetration depth. When uniform lateral confinement is considered, the compressive strength can be derived as

$$f'_c = \left(\frac{2}{3} - \frac{2}{9} \tan \theta \right) f_c + \left(1 + \frac{2 \tan \theta}{3} \right) P_H \quad (1)$$

where f_c is the unconfined uniaxial compression strength; P_H is the applied hydrostatic pressure; θ is the frictional angle which was found to be 50° for concrete.

In this test, the confinement of concrete by steel lining leads to the increase of target compression strength which is useful for the penetration resistance. Many tests indicated that for concrete-like materials a small lateral confining pressure in the order of 10% of the quasi-static uniaxial compressive strength can increase the axial compressive strength by as much as 50%. With the increase of lateral confining pressure the behavior of the loaded specimen gradually becomes more ductile, leading to an eventual transition from brittle failure to ductile response [21].

Fig. 6 shows the depths of penetration of UHPC on different times of penetration. The depth of M2 is biggest and that of

M2SF3BF1 is smallest on the first time of penetration. The penetration depths of the targets with coarse aggregates are bigger than those of the targets without coarse aggregates on the first time of penetration. On the contrary, the penetration depths of the targets with coarse aggregates are smaller than those of the targets without coarse aggregates on the second time of penetration. Results show that coarse aggregates have better effect on the resistance of UHPC to repeated penetration. The target of M2SF3BF1 was

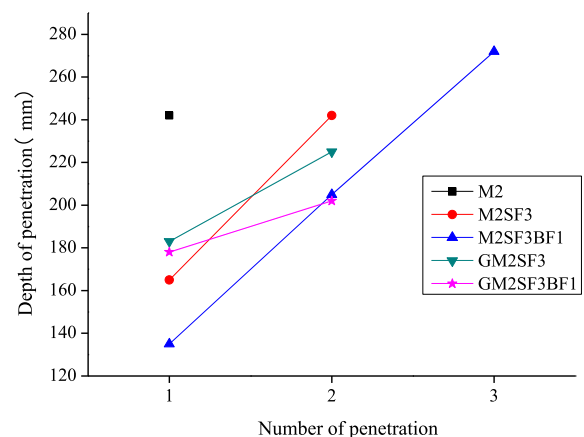


Fig. 6. Depth of penetration of UHPC on different number of penetration.

subjected to penetration for three times and the results show that the penetration depth increases linearly with the number of impact.

Fig. 7 shows the penetration of target M2 by the high-speed camera. There were crushed concretes and huge fire when bullets impacted on the targets. The spray of concrete pieces was seen from the pictures of the high-speed camera. Fire appeared because of the high temperature in the initial stage and the funnel-shaped crater also appeared on the front surface. Many concrete pieces with different sizes, mass and shapes appeared near the target. The size and number of the sprayed concrete pieces were decreased by fiber reinforcement. The bullet of the second penetration went into the crater of the first penetration so the sprayed concrete pieces on the second penetration were obviously less than those on the first penetration.

3.2. Damage of UHPC targets subjected to repeated penetration

The damage of UHPC targets was measured by the ultrasonic wave velocity method [22]. The ultrasonic wave velocities of different targets before and after penetration were measured. The damage of concrete target after each time of penetration, D_n is defined as:

$$D_n = 1 - v_n^2 / v_0^2 \quad (2)$$

where, D_n is the damage of concrete targets subjected to the n -th penetration, v_n (km/s) is the average ultrasonic wave velocity of the target subjected to the n -th penetration, v_0 (km/s) is the average ultrasonic wave velocity of the initial target before penetration.

Four points were selected for measuring the ultrasonic wave velocity around the middle crater on the target and the average

ultrasonic wave velocity was calculated using the four measuring data. The ultrasonic wave velocity is equal to the thickness of the target divided by time of the ultrasonic wave transmitting through the thickness. The four points were directly above, direct below, on the left and on the right of the middle crater respectively. The selected points must be kept away from the concrete cracks or spalling. The ultrasonic wave velocity could not be measured and the damage was set as one if the concrete target was damaged severely.

The average ultrasonic wave velocity and damage of concrete target are shown in Table 5. The wave velocities of different targets decreased obviously after the penetration but the decreasing degree was different as shown in Table 5. The variety in the changing of the wave velocity shows the different abilities of UHPC targets against repeated penetration. The decreasing of the wave velocity of the target M2SF3BF1 is the least after two times of penetration which proves its best resistance to penetration. The damage of the target M2SF3BF1 is smallest and that of the target GM2SF3BF1 is biggest after the first penetration. The damage of the target M2SF3BF1 is still smallest and that of the target GM2SF3 becomes biggest after the second penetration. So the ability of the target M2SF3BF1 against repeated penetration is the best on the point of the damage.

4. Results and analysis of different depth explosion

4.1. Explosion damage and explosion crater of concrete targets

The placing depth of TNT explosive has great influence on the damage characteristics of concrete targets. The front sides of the concrete targets with 150 mm placing depth of TNT were completely destroyed and only half part of each target remained. On the other hand, the relative regular craters were found in the

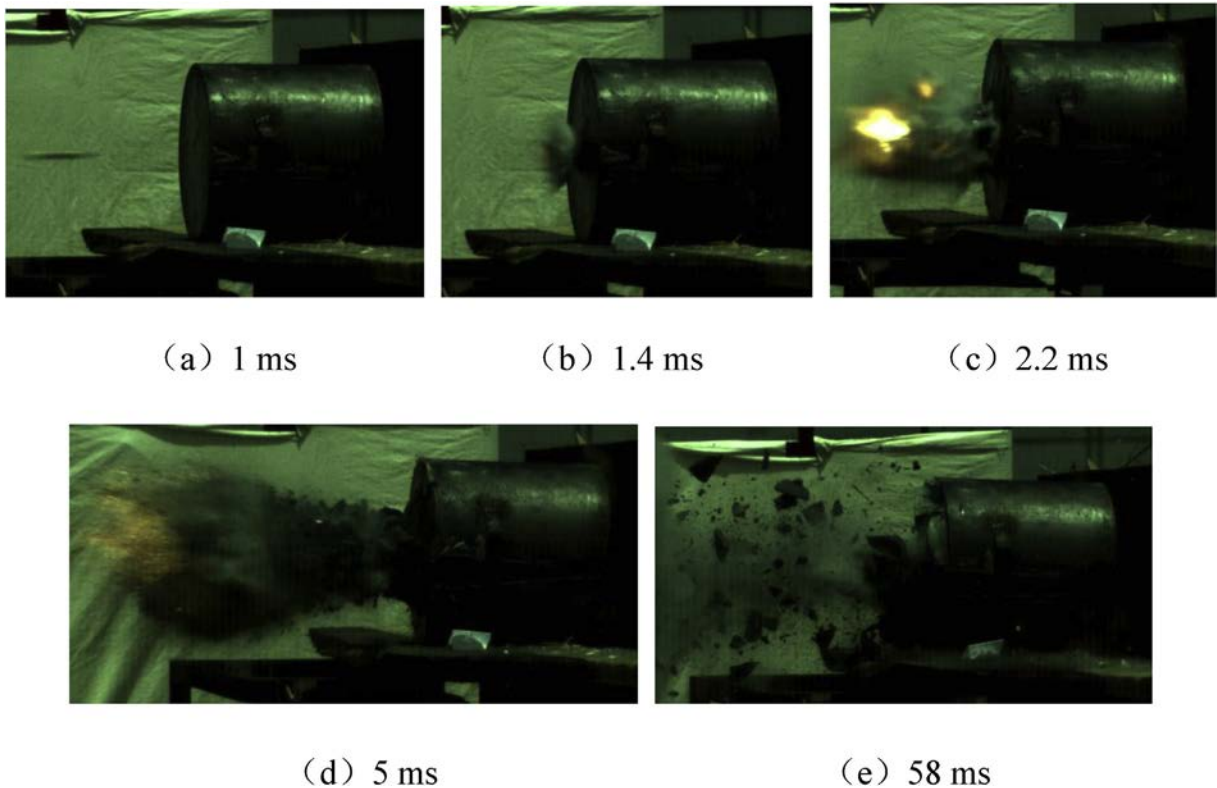


Fig. 7. Penetration process of target M2 by high-speed camera.

Table 5
Calculation results of the damage of UHPC targets.

Materials of targets	v_0 (km/s)	v_1 (km/s)	D_1	v_2 (km/s)	D_2
M2	4.7	Crushed and cannot be measured	–	–	–
M2SF3	4.6	4.0	0.226	3.37	0.465
M2SF3BF1	4.5	4.4	0.065	3.60	0.383
GM2SF3	4.8	4.0	0.303	2.20	0.797
GM2SF3BF1	4.8	3.2	0.545	Cracked heavily and cannot be measured	–

Note: D_1 , D_2 are the damages of targets after the first and second penetration respectively which are calculated using Eq. (2).

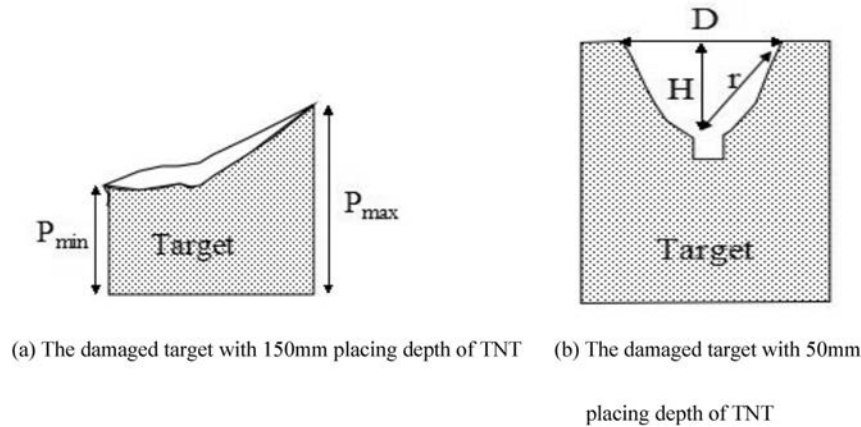


Fig. 8. The schematic diagram of concrete targets after the explosion.

front sides of the concrete targets with 50 mm placing depth of TNT. Therefore, two kinds of parameters are used to measure the damages of concrete targets. The former is described by the target residual height P and the latter is described by the size of the explosion crater. Fig. 8 shows the schematic diagram of concrete targets after the explosion. P_{max} is the maximum target residual height and P_{min} is the minimum target residual height. D is the caliber of the explosion crater and r is the radius of the explosion crater. H is the depth of the explosion cavity. The related explosion test data are shown in Tables 6 and 7.

The extent of concrete damage was characterized objectively by the parameters in Tables 6 and 7. The explosion resistance of concrete target M2 without fiber was very weak. The M2 targets were

destroyed severely regardless of the mass of TNT explosive. The only difference is that No.1 target (M2) was broken into uniform small particles while No.2 target (M2) was broken into some big pieces. The results are caused by the essential characteristics of the matrix of UHPC which is very brittle. The target M2 without adding any fibers could not resist the strong stress and was broken uniformly owing to stress wave which generated high compressive and shear force in the targets.

It is found that the placing depth of TNT explosive is an important factor which results in various degrees of damage comparing the explosion results of No.3 target (M2SF3), No.5 target (M2SF3BF1) and No.7 target (GM2SF3). The above three kind of targets have small differences in static compressive strength. The

Table 6
The explosion test results of concrete targets with 150 mm placing depth of TNT.

Number order (No.)	Materials of targets	m_{TNT} (g)	Dimension of TNT(mm)	P_{max} (mm)	P_{min} (mm)	The damage results
1	M2	150	$\Phi 37 \times 90$			The target is broken into small particles
3	M2SF3	50	$\Phi 37 \times 30$	170	35	There are 3 large cracks and a large number of small cracks on the rear side
5	M2SF3BF1	25	$\Phi 37 \times 15$	210	92	There are only a few cracks on the rear side
7	GM2SF3	25	$\Phi 37 \times 15$	300	0	The target is torn along the axial direction and the rear side is seriously damaged

Table 7
The explosion test results of concrete targets with 50 mm placing depth of TNT.

Number order (No.)	Materials of targets	m_{TNT} (g)	Dimension of TNT(mm)	r (mm)	H (mm)	D (mm)		The damage results
						D_{max}	D_{min}	
2	M2	25	$\Phi 37 \times 15$					The target is broken into some big pieces
4	M2SF3	25	$\Phi 37 \times 15$	90	48.5	290	220	There are 6 large cracks on the front side
6	M2SF3BF1	25	$\Phi 37 \times 15$	89	45	220	150	There are 7 large cracks on the front side
8	GM2SF3	25	$\Phi 37 \times 15$	78	36	250	140	There are 6 large cracks on the front side and a penetrating crack through the body

Notes: H and r are the average value of the measured data.

TNT quantity of No.3 target is two times compared with No.5 target and No.7 target. However the target residual height of No.3 target reduced much lower and a lot of small flaws appeared in the rear side of the target. The TNT quantity and buried depth of No. 4 target (M2SF3), No.6 target (M2SF3BF1) and No.8 target (GM2SF3) are the same and the explosion craters were formed in the front side of these targets. The explosion resistance of the three kinds of targets can be characterized well by the size of explosion craters.

The data show that No.8 target had the minimum size of explosion crater including the depth of the blasting crater and the radius of the explosion crater. However, the penetrating cracks had been found in No.8 target and the number of cracks on the front side was the biggest in all targets. There are coarse aggregates in No. 8 target which are effective for the increase of compressive strength and have small effect in the improvement of tensile strength. At the same time, coarse aggregates cause the nonuniformity in the concrete structure which results in stress concentration. The dimension of the explosion crater of No.6 target was smaller than that of No.4 target and the state of target M2SF3BF1 was preserved much better. The results are due to the synergistic effect of hybrid fibers which can increase the tensile and bending strength of No.6 target reinforced by basalt fibers and steel fibers. The explosion resistance of M2SF3BF1 is the best by comparing the test results in Tables 6 and 7.

From the results we can see that: (1) The explosion resistance of concrete matrix without any reinforcement is weak. (2) The quantity of the explosive and the placing depth of TNT are two important factors which have obvious influence on the damage of concrete target. The more deeply is the TNT explosive placed, the more severe is the concrete damage. (3) The explosion resistance of the concrete is closely linked with the composition and the

structure of the target material. The concrete of high explosion resistance not only has high compressive strength, but also has excellent tensile and shear strength.

4.2. Fracture pattern of concrete targets subjected to explosion

Two groups of targets have entirely different fracture characteristics because of the different placing depth of TNT in the explosion tests. The two groups are discussed separately according to the different depths of TNT explosives. The fracture pattern and crater feature of concrete target are shown in Fig. 9 and 10.

As shown in Figs. 9 and 10, the concrete targets with 150 mm placing depth of TNT were destroyed severely due to the blast shock wave from the sudden release of explosive energy. The large energy can not be timely released to the air when the placing depth is deep enough which impedes the propagation of the blast shock wave. Then the air temperature and blast shock wave pressure in the concrete target rise sharply. Various reflected shock wave and transmitted wave are generated gradually. These waves and the flow air are combined together to form a flow field which is coupling with the concrete structure. High compressive stress and shear stress are generated by the fluid-structure coupling effect which causes great damages in concrete targets. The explosion damages of concrete targets with 50 mm placing depth of TNT were relatively light. The craters were formed on the front sides of the concrete targets except No.2 target (M2). The shock wave energy can be dissipated quickly into the air when the TNT placing depth is small and the fluid-structure coupling effect decreases a lot. Parts of the reflected and transmitted waves are converted into seismic waves and the forces in the concrete targets especially the shear and tensile stresses are reduced.

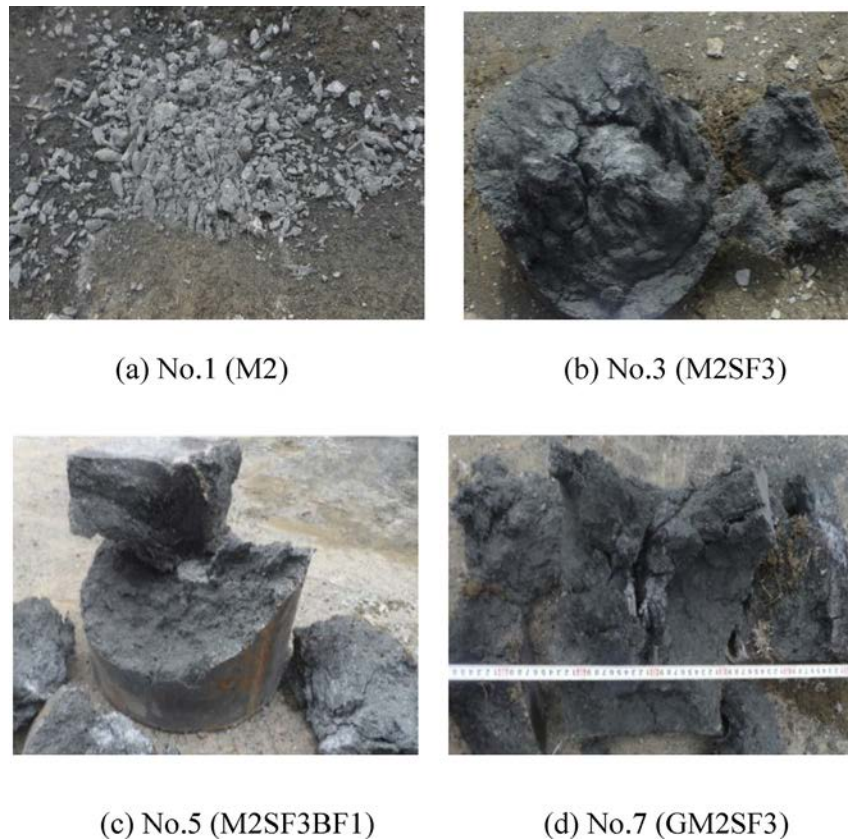


Fig. 9. The fracture pattern of concrete targets with 150 mm placing depth of TNT.

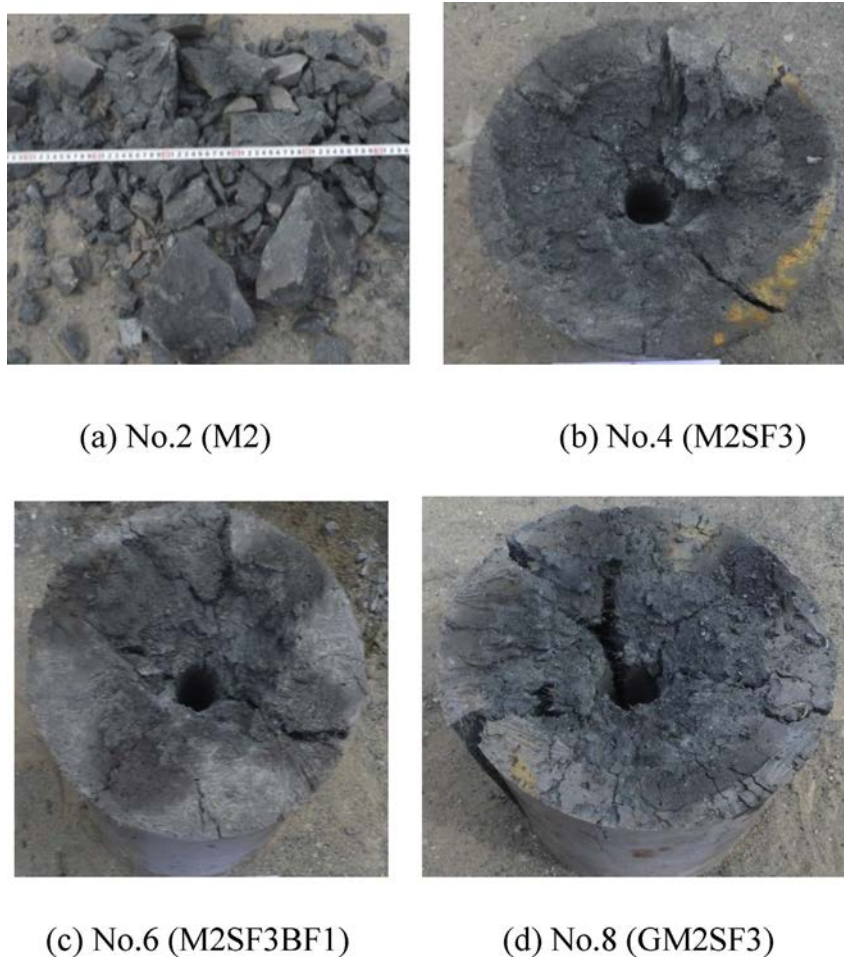


Fig. 10. The damage results of concrete targets with 50 mm placing depth of TNT.

The reference concrete M2 without any fiber or coarse aggregate is a brittle material and is unable to resist the large compressive, tensile and shear forces by the blast overpressure. So Target M2 was destroyed most severely and was broken into small particles. The other three kinds of targets had relatively less damages. These three kinds of targets with fiber reinforcement have the static compressive strength over 200 MPa. It is found from Fig. 9 that the residual volume of No.5 target (M2SF3BF1) was the largest and big concrete parts of No.3 target (M2SF3) and No.7 target (GM2SF3) were thrown into the air. As seen from Fig. 10, complete funnel crater were formed in the three groups of fiber reinforced UHPC targets. Results show that the crater volume of No.8 target (GM2SF3) is the minimum and that of No.4 target (M2SF3) is the maximum. However, the crater volume does not completely represent the explosion resistance of concrete targets. For example, the crater volume of No.8 target (GM2SF3) is the minimum while its explosion resistance is obviously weaker than that of target M2SF3BF1 or M2SF3 because the penetrating cracks passed through the whole body of No.8 target.

The No.6 target (M2SF3BF1) was prepared by adding basalt fibers on the basis of No.4 target (M2SF3). Basalt fiber is a kind of inorganic nonmetallic fiber with high modulus of elasticity. The mixture of basalt fiber and steel fiber can optimize the internal structure of concrete and improve the static mechanical properties of concrete target. The static mechanical test has already confirmed this point. The No.8 target (GM2SF3) was prepared by adding coarse basalt aggregates on the basis of No. 4 target (M2SF3). But

the coarse basalt aggregates contribute little on the increase of concrete explosion resistance. One reason is that coarse aggregates are only beneficial to the improvement of the compressive strength of concrete and have small effect on the increasing of fracture energy. Another reason is that coarse aggregates decrease the uniformity and increase the internal stress concentration in concrete structure. So target M2SF3BF1 has the best explosion resistance based on the tests and analysis.

4.3. Numerical simulation of UHPC subjected to explosion

A large number of nonlinear transient dynamic problems are involved in the process of explosion. The numerical simulation is introduced as an important research method in order to describe accurately the mechanism of UHPC subjected to explosion.

4.3.1. Finite element model

The fracture process of UHPC subjected to blasting was simulated by using the nonlinear finite element software ANSYS/LS-DYNA. To simplify the analysis, a quarter of target model was selected according to the actual target dimension. The TNT explosive and concrete target were meshed by using three dimensional entity unit SOLID164. The cylindrical concrete model has the radius of 150 mm and the height of 300 mm. The size of the hole for placing explosive is $\Phi 38$ mm \times 150 mm and the size of TNT explosive is $\Phi 37$ mm \times 15 mm. The remaining space in the hole is air. The computational grids near the TNT explosive were meshed



Fig. 11. Finite element model.

finely to ensure the calculation precision. The finite element model is shown in Fig. 11. The system of units is cm-g-μs.

4.3.2. Material model and equation of state

The material model of TNT explosive is *MAT_HIGH_EXPLOSIVE_BURN. The density of TNT is 1640 kg/m³ and the detonation velocity is 6930 m/s. The equation of state of TNT explosive is *EOS_JWL shown in Eq. (3) and the JWL parameters are shown in Table 8 [23]:

$$p = A \left(1 - \frac{\omega}{R_1 V} \right) e^{-R_1 V} + B \left(1 - \frac{\omega}{R_2 V} \right) e^{-R_2 V} + \frac{\omega E}{V} \quad (3)$$

where, A and B are linear explosion parameters. ω , R_1 and R_2 are nonlinear explosion parameters. p is pressure, V is relative volume, E is internal energy and e is mathematical constant.

The material model of concrete is *MAT_JOHNSON_HOLMQUIST_CONCRETE shown in Eq. (4) [23].

$$\sigma^* = [A(1 - D) + BP^{*N}] \times [1 - c \ln(\dot{\epsilon}^*)] \quad (4)$$

where, $\sigma^* = \sigma/f_c$ is normalized equivalent stress, σ is the actual equivalent stress, and f_c is the quasi-static uniaxial compressive strength. D is the damage parameter, A and B are the coefficients of the model, c is the influence coefficient of strain rate, N is pressure hardening index. $P^* = P/f_c$ is the normalized pressure and $\dot{\epsilon}^* = \dot{\epsilon}/\dot{\epsilon}_0$ is the dimensionless strain rate. The model accumulates damage both

Table 8
Parameters of JWL equation for TNT explosive.

A(GPa)	B(GPa)	R1	R2	ω	$E_0(\text{cm}^2/\mu\text{s}^2)$	V_0
374	3.23	4.15	0.95	0.35	0.07	1.00

Note: E_0 is initial internal energy; V_0 is initial relative volume.

Table 9
Parameters of HJC model for UHPC (M2SF3).

$\rho(\text{kg/m}^3)$	G(GPa)	A	B	C	N	$f_c(\text{MPa})$	T(MPa)	EPS_0	$\epsilon_{f\text{min}}$
2440	22	0.79	1.6	0.007	0.61	200	4	10^{-6}	0.004
S_{max}	$P_{\text{crush}}(\text{MPa})$	μ_{crush}	$P_{\text{lock}}(\text{GPa})$	μ_{lock}	D_1	D_2	$K_1(\text{GPa})$	$K_2(\text{GPa})$	$K_3(\text{GPa})$
7.0	83	0.66	1	0.08	0.04	1.0	85	-171	208

Notes: EPS_0 -Reference strain rate, $\epsilon_{f\text{min}}$ -Amount of plastic strain before fracture, S_{max} -Normalized maximum strength.

from the equivalent plastic strain and plastic volumetric strain, and is expressed as

$$D = \sum \frac{\Delta\epsilon_p + \Delta\mu_p}{D_1(P^* + T^*)^{D_2}} \quad (5)$$

where, $\Delta\epsilon_p$ and $\Delta\mu_p$ are the equivalent plastic strain and plastic volumetric strain, D_1 and D_2 are material constants and $T^* = T/f_c$ is the normalized maximum tensile hydrostatic pressure.

The pressure for fully dense material is expressed as

$$P = K_1 \bar{\mu} + K_2 \bar{\mu}^2 + K_3 \bar{\mu}^3 \quad (6)$$

where, K_1 , K_2 and K_3 are material constants and modified volumetric strain is defined as

$$\bar{\mu} = \frac{\mu - \mu_{\text{lock}}}{1 + \mu_{\text{lock}}} \quad (7)$$

where, μ_{lock} is the locking volumetric strain.

The JHC model parameters of target M2SF3 are listed in Table 9. The parameters of M2SF3 are obtained from the references [24,25] and modified according to relevant static and blast experiments.

The material model of air is *MAT_NULL. The equation of state of air is *EOS_LINEAR_POLYNOMIAL which is a linear polynomial equation shown in Eq. (8) and the model parameters are shown in Table 10 [23].

$$P = C_0 + C_1 \mu + C_2 \mu^2 + C_3 \mu^3 + (C_4 + C_5 \mu + C_6 \mu^2) E \quad (8)$$

$$\mu = \frac{\rho}{\rho_0} - 1 \quad (9)$$

where, P is pressure. C_0 , C_1 , C_2 , C_3 , C_4 , C_5 and C_6 are the coefficients of the polynomial equation. E is internal energy and ρ/ρ_0 is the ratio of current density to initial density.

4.3.3. Results of finite element simulation

The material control algorithm was set in the solver after the preprocessing operation. Both the TNT explosive and air were modeled with Euler meshes and computed with multi-material ALE algorithm. Air and TNT explosive models were regarded as fluid and formed a multi material combination ALE_MULTI_MATERIAL_GROUP. The concrete target was modeled with Lagrangian meshes and was regarded as solid. Then separate type models were combined into a whole by the fluid-solid coupling method. The result files were processed by LS-PREPOST software after the computation and the fracture process of the concrete target was obtained as shown in Fig. 12.

Fig. 12 shows the whole damage pattern of target M2SF3 subjected to explosion. The process of expansion and the forming of concrete blasting crater are well simulated. The size of blasting crater is estimated by using graphical tools of the software and the simulation results are as follows: (1) The simulation value of funnel mouth diameter D is 240 mm; (2) The simulation value of the

Table 10
Parameters of the model of air.

$\rho_0(\text{kg/m}^3)$	C0	C1	C2	C3	C4	C5	C6	$E_0(\text{MPa})$	V_0
1.290	0	0	0	0	0.4	0.4	0	0.25	1.0

Note: E_0 is initial internal energy; V_0 is initial relative volume.

blasting cavity depth H is 60 mm which is slightly larger than the test value; (3) The simulation value of the explosion crater radius is 100 mm. Some simulation results are slightly larger than the test values but in the range of experiment error.

The simulation results can show some physical phenomena which are difficult to be observed and measured. The air below the TNT explosive was subjected to high compressive stress which made the concrete hole damaged severely. A smaller size of the blasting crater was found below the position of TNT explosive. The target presented double craters in the section plan which was the result of explosion shock waves.

The explosion shock wave can lead to very strong overpressure especially in the central region of explosion and this value can be obtained accurately by means of numerical simulation. In order to get the characteristics of pressure distribution and the attenuation rule of explosion shock wave, the pressure data were collected from six elements with the same grid spacing from near to far from the position of TNT explosive. The six elements are shown in Fig. 13 and

the distances from the explosive are 15, 30, 45, 60, 75 and 90 mm respectively.

From Fig. 13 we can see that the pressure of explosion shock wave decreases gradually with the increase of distance from the explosive center. The sharpest pressure-time curve appeared in the nearest element with the maximum pressure up to 12.5 GPa and the concrete material was broken instantly here. Then the pressure decreased fast. The pressure of the element in Fig. 13(b) is only 4.7 GPa and the reduction percentage is 62.4% compared to the previous element. The reduction percentage of the other elements compared with the previous element is 97%, 83.3%, 40% and 26.7% respectively from near to far from the TNT explosive. The simulation results show the action of explosion shock wave. The target materials near explosion field were completely destroyed. The pressure of shock wave decayed rapidly and the target materials far from the blasting area were damaged lightly.

The propagation characteristics of explosion shock wave lead to different damage patterns of target materials. The explosion shock wave is the comprehensive effect of various forms of waves including incident wave, reflected wave and transmitted wave. Several kinds of waves with different properties are superposed together which leads to different damage effects of different parts of concrete target. The targets suffer from multiple failure types including tensile, compressive and shear failure for the change of wave propagation characteristics.

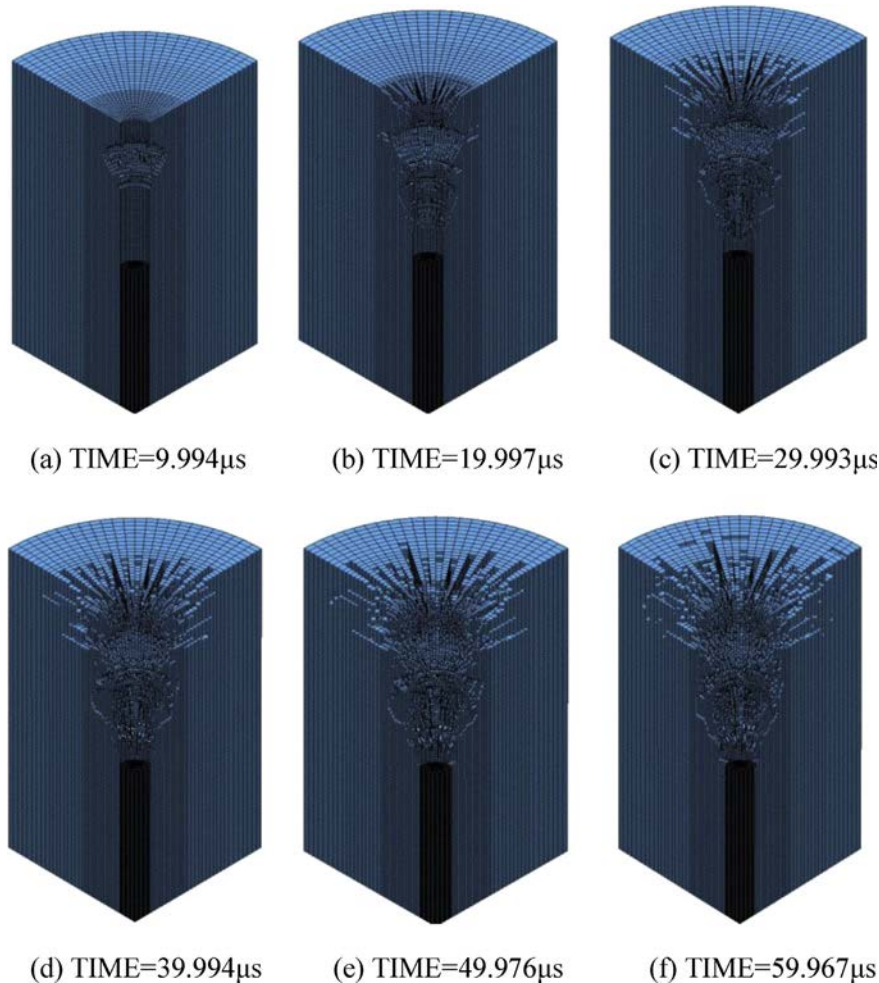


Fig. 12. The fracture process of the concrete target (M2SF3) subjected to explosion by simulation.

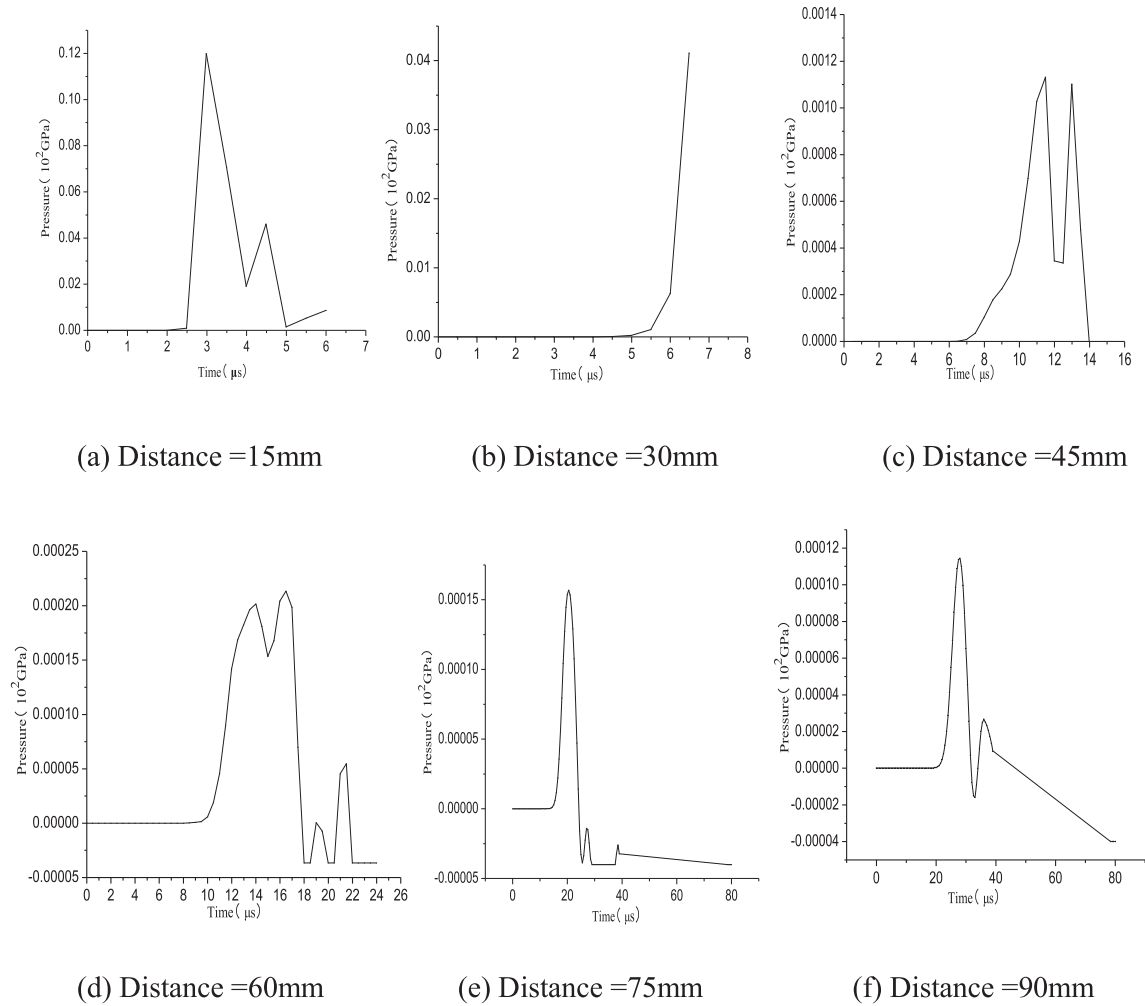


Fig. 13. The pressure-time curve of different elements with different distance from the explosive.

The comprehensive mechanical properties of UHPC should be improved in order to increase its explosion resistance. Not only the compressive strength but also the flexural and shear strength should be enhanced. The one sided enhancement of UHPC properties can hardly lead to the improvement of blast resistance. It has been proved by the hybrid fiber reinforced target M2SF3BF1 which has the best explosion resistance.

5. Conclusions

The dynamic behavior of UHPC was researched subjected to repeated penetration and different depth explosion. The resistance of UHPC to penetration and explosion is improved significantly by hybrid fiber reinforcement. The penetration depth and damage of concrete target increased with the number of penetration. The mass and the placing depth of explosive have important effects on the damage and fracture of concrete target. The penetration process of UHPC was observed by the high-speed camera and the explosion process of UHPC was simulated by the finite element method. The main findings of the research are as follows:

(1) The penetration resistance of UHPC was improved with the help of steel fibers and basalt coarse aggregates which makes the targets to resist two times of impact of bullets. The size

and number of cracks in the target without coarse aggregates are much smaller than those in the target with coarse aggregates. The target M2SF3BF1 with both steel fibers and basalt fibers can resist three times of penetration and shows excellent ability against impact.

- (2) The penetration depths of the targets with coarse aggregates are smaller than those of the targets without coarse aggregates on the second time of penetration. Results show that coarse aggregates have better effect on the resistance to repeated penetration. The increase of the penetration depth is 46.7%, 51.8%, 23.0%, 13.5% respectively for M2SF3, M2SF3BF1, GM2SF3, GM2SF3BF1 on the second penetration. The penetration depth of the target M2SF3BF1 increased linearly with the number of impact.
- (3) The confinement of the steel line leads to the increase of target compression strength which is useful for the resistant to penetration. The size and number of the sprayed concrete pieces were decreased by fiber reinforcement and the sprayed concrete pieces on the second penetration were obviously less than those on the first penetration. The decrease of wave velocity of target M2SF3BF1 is the least after two times of penetration which proves its best resistance to repeated penetration.
- (4) The more are the TNT mass and placing depth, the more severe is the target damage. The concrete targets with

150 mm placing depth of TNT were destroyed completely and only half of the target body remained while the concrete targets with 50 mm placing depth of TNT had relatively smaller damage and regular craters in the front sides.

- (5) The comprehensive mechanical properties of UHPC should be considered to improve the explosion resistance of concrete target. The target materials would have strong explosion resistance when basalt fibers and steel fibers were mixed together because of the synergistic effect between the fibers.
- (6) The process of UHPC subjected to blasting was simulated well by using the nonlinear finite element method. The simulation size of blasting crater of target M2SF3 is 240 mm, 60 mm and 100 mm for diameter, cavity depth and crater radius which are close to the experimental data. The simulation results show that the pressure of explosion shock wave decreases gradually with the increase of distance from the explosive center. The propagation characteristics of explosion shock wave lead to multiple failure modes which include tensile, compressive and shear failure of targets.

Acknowledgments

This work is supported by the National Natural Science Foundation of China (No.51278249, 50808101).

References

- [1] Forrestal MJ, Tzou DY. A spherical cavity-expansion penetration model for concrete targets. *Int J Solids Struct* 1997;34:4127–46.
- [2] Gomez JT, Shukla A. Multiple impact penetration of semi-infinite concrete. *Int J Impact Eng* 2001;25:965–79.
- [3] Almansa EM, Canovas MF. Behaviour of normal and steel fiber-reinforced concrete under impact of small projectiles. *Cem Concr Res* 1999;29:1807–14.
- [4] Teng TL, Chu YA, Chang FA, Chin HS. Simulation model of impact on reinforced concrete. *Cem Concr Res* 2004;34:2067–77.
- [5] Almusallam TH, Siddiqui NA, Iqbal RA, Abbas H. Response of hybrid-fiber reinforced concrete slabs to hard projectile impact. *Int J Impact Eng* 2013;58:17–30.
- [6] Tabatabaei ZS, Volz JS, Baird J, Gliha BP, Keener DI. Experimental and numerical analyses of long carbon fiber reinforced concrete panels exposed to blast loading. *Int J Impact Eng* 2013;57:70–80.
- [7] Zhou XQ, Kuznetsov VA, Hao H, Waschl J. Numerical prediction of concrete slab response to blast loading. *Int J Impact Eng* 2008;35:1186–200.
- [8] Yu R, Spiesz P, Brouwers HJH. Mix design and properties assessment of ultra-high performance fibre reinforced Concrete (UHPRFC). *Cem Concr Res* 2014;56:29–39.
- [9] Wang W, Liu J, Agostini F, Davy CA, Skoczylas F, Corvez D. Durability of an ultra high performance fiber reinforced Concrete (UHPRFC) under progressive aging. *Cem Concr Res* 2014;55:1–13.
- [10] Habel K, Viviani M, Denarie E, Bruhwiler E. Development of the mechanical properties of an ultra-high performance fiber reinforced Concrete (UHPRFC). *Cem Concr Res* 2006;36:1362–70.
- [11] Oertel T, Helbig U, Hutter F, Klettl H, SEXTL G. Influence of amorphous silica on the hydration in ultra-high performance concrete. *Cem Concr Res* 2014;58:121–30.
- [12] Tuan NV, Ye G, Breugel KV, Copuroglu O. Hydration and microstructure of ultra high performance concrete incorporating rice husk ash. *Cem Concr Res* 2011;41:1104–11.
- [13] Kang ST, Kim JK. The relation between fiber orientation and tensile behavior in an ultra high performance fiber reinforced cementitious composites (UHPRFC). *Cem Concr Res* 2011;41:1001–14.
- [14] Millard SC, Molyneux TCK, Barnett SJ, Gao X. Dynamic enhancement of blast-resistant ultra high performance fibre-reinforced concrete under flexural and shear loading. *Int J Impact Eng* 2010;37:405–13.
- [15] Maca P, Sovjak R, Konvalinka P. Mix design of UHPRFC and its response to projectile impact. *Int J Impact Eng* 2014;63:158–63.
- [16] Riedel W, Noldgen M, Straßburger E, Thoma K, Fehling E. Local damage to ultra high performance Concrete structures caused by an impact of aircraft engine missiles. *Nucl Eng Des* 2010;240:2633–42.
- [17] Ellis BD, Dipaolo BP, McDowell DL, Zhou M. Experimental investigation and multiscale modeling of ultra-high- performance concrete panels subject to blast loading. *Int J Impact Eng* 2014;69:95–103.
- [18] Yi NH, Kim JHJ, Han TS, Cho YG, Lee JH. Blast-resistant characteristics of ultra-high strength concrete and reactive powder concrete. *Constr Build Mater* 2012;28:694–707.
- [19] Mao L, Barnett S, Begg D, Schleyer G, Wight G. Numerical simulation of ultra high performance fibre reinforced concrete panel subjected to blast loading. *Int J Impact Eng* 2014;64:91–100.
- [20] Elshenawy T, Li QM. Influences of target strength and confinement on the penetration depth of an oil well perforator. *Int J Impact Eng* 2013;54:130–7.
- [21] Mu ZC, Dancygier AN, Zhang W, Yankelevsky DZ. Revisiting the dynamic compressive behavior of concrete-like materials. *Int J Impact Eng* 2012;49:91–102.
- [22] Lai JZ, Sun W. Dynamic behaviour and visco-elastic damage model of ultra-high performance cementitious composite. *Cem Concr Res* 2009;39:1044–51.
- [23] LSTC. LS-DYNA keyword user's manual, version970. California: Livermore Software Technology Corporation; 2003. 13.4–13.6, 20.350–20.352.
- [24] Polanco-Loria M, Hopperstad OS, Borvik T, Berstad T. Numerical predictions of ballistic limits for concrete slabs using a modified version of the HJC concrete model. *Int J Impact Eng* 2008;35:290–303.
- [25] Lai JZ, Sun W, Xu S, Yang CM. Dynamic properties of reactive powder Concrete subjected to repeated impacts. *ACI Mater J* 2013;110:463–72.